AGU PUBLICATIONS

Geochemistry, Geophysics, Geosystems

RESEARCH ARTICLE
10.1002/2016GC006553

Key Points:
- Long-chain unsaturated alkenones and *n*-alkanes thermally mature at short time scales relevant to geologic processes such as seismic slip
- We determine the kinetics of biomarker thermal maturation, which can be used to model heating at high temperatures and short time scales
- Alkenones thermally mature at temperatures as low as 100°C, which could affect paleoclimatological signals from heated samples

Supporting Information:
- Supporting Information S1
- Figure S1
- Figure S2
- Figure S3
- Figure S4
- Figure S5
- Figure S6
- Figure S7
- Table S1
- Table S2
- Table S3

Correspondence to:
H. S. Rabinowitz,
hannahr@ldeo.columbia.edu

Citation:
Rabinowitz, H. S., P. J. Polissar, and H. M. Savage (2017), Reaction kinetics of alkenone and *n*-alkane thermal alteration at seismic timescales, *Geochem. Geophys. Geosyst.*, *18*, doi:10.1002/2016GC006553.

Received 25 JUL 2016
Accepted 31 DEC 2016
Accepted article online 7 JAN 2017

Reaction kinetics of alkenone and *n*-alkane thermal alteration at seismic timescales

H. S. Rabinowitz[1,2], P. J. Polissar[1], and H. M. Savage[1]

[1]Lamont-Doherty Earth Observatory, Palisades, New York, USA, [2]Department of Earth and Environmental Science, Columbia University, New York, New York, USA

Abstract Recent experiments and field observations have indicated that biomarker molecules can react over short timescales relevant to seismic slip, thereby making these compounds a useful tool in studying temperature rise in fault zones. However, short-timescale biomarker reaction kinetics studies have previously focused on compounds that have already experienced burial heating. Here, we present a set of hydrous pyrolysis experiments on Pleistocene-aged shallow marine sediment to develop the reaction kinetics of long-chain alkenone destruction, change in the alkenone unsaturation ratio ($U^{k'}_{37}$), and change in the *n*-alkane chain length distribution. Our results show that biomarker thermal maturity provides a useful method for detecting temperature rise in the shallow reaches of faults, such as subduction zone trench environments. Through the course of our work, we also noted the alteration of total alkenone concentrations and $U^{k'}_{37}$ values in crushed sediments stored dry at room temperature for durations of months to years but not in the solvent extracts of these materials. This result, though parenthetical for our work in fault zones, has important implications for proper storage of sedimentary samples to be used for alkenone paleotemperature and productivity analysis.

1. Introduction

The distribution and structure of organic molecules (biomarkers) evolves in measurable ways when sediments are heated over a range of timescales and temperatures. Thermal maturity of organic molecules has long been studied in applications related to petroleum generation, which usually occurs on the scale of millions of years [*Peters et al*., 2004]. Only recently has biomarker thermal maturity over very short timescales been experimentally investigated [*Sheppard et al*., 2015]. The kinetics of biomarker maturation at short timescales are an important tool for constraining the temperature rise in sediments exposed to short duration heat sources such as earthquakes, forest fires, bolide impacts, dike intrusions, and hydrothermal fluids [*Bishop and Abbott*, 1993; *Bowden et al*., 2008; *Kaiho et al*., 2013; *Parnell et al*., 2010, 2005; *Polissar et al*., 2011; *Savage et al*., 2014; *Schimmelmann et al*., 2009; *Simoneit*, 1994; *Simoneit et al*., 1994]. In this paper, we focus on thermal alteration from earthquakes, but our results are applicable to other environments as well.

Temperature rise during earthquakes is a function of the absolute fault shear stress during sliding. However, determining earthquake temperature rise from the rock record has proven difficult. At shear stress values on the order of 10–100 MPa (typical values within the seismogenic zone), temperature rise could easily reach several hundred to over 1000°C during large earthquakes, which is hot enough to melt rock. Some faults have unequivocally experienced such significant temperature rises, and can be identified by the presence of frictional melt known as pseudotachylyte [e.g., *Sibson*, 1975]. Pseudotachylyte in faults, however, is not ubiquitous and its absence in most faults raises the difficult question: why did the fault not get hot enough to melt? One possibility is that pseudotachylyte does not preserve well in the rock record, retrograding to minerals such as micas that make it difficult to pinpoint their earthquake-related origins [*Kirkpatrick and Rowe*, 2013; *Rowe and Griffith*, 2015]. Another possibility is that earthquakes generally do not produce sufficiently large temperature excursions to melt fault rocks. A range of dynamic weakening mechanisms such as pore fluid pressurization, flash heating, and mineral dehydration, have been documented in laboratory experiments [e.g., *Collettini et al*., 2013; *Di Toro et al*., 2011; *Han et al*., 2007; *Mase and Smith*, 1985; *Rice*, 2006] and provide ways to reduce the effective shear stress on a fault during dynamic slip, thus limiting the temperature rise on the fault over the course of a seismic event. However, it is not well understood how effective these mechanisms may be in real faults.

Other methods have been developed more recently to investigate the subsolidus coseismic temperature rise on a fault, such as thermally dependent alterations to the smectite structure, decarbonation of the fault host rocks, changes in the magnetic signatures of frictionally heated sediments, and fission-track thermochronology [*d'Alessio et al*., 2003; *Hirono et al*., 2007; *Rowe and Griffith*, 2015; *Schleicher et al*., 2015; *Yang et al*., 2016]. Additionally, organic thermal maturity is becoming an established paleoseismic indicator that can be applied to faults hosted in sedimentary rocks. Field studies of the thermal maturity of organic material have considered vitrinite reflectance [*Barker and Pawlewicz*, 1986; *Burnham et al*., 1989; *Fulton and Harris*, 2012; *Sakaguchi et al*., 2011], as well as molecular methods focusing on a range of biomarkers [*Polissar et al*., 2011; *Savage et al*., 2014].

Previous studies of biomarker thermal maturity have focused on faults hosted in moderate to deeply buried rocks where the suite of biomarkers useful for paleoseismic thermal maturity studies reflect a relatively high background thermal maturity (e.g., methylphenanthrenes and diamondoids) [*Polissar et al*., 2011; *Savage et al*., 2014; *Sheppard et al*., 2015]. In order to apply biomarkers as a fault thermometer in shallow sediments that have not experienced burial heating (such as would be expected in faults located within the shallowest portions of subduction zones that determine tsunamigenic potential), it is necessary to determine the kinetics of thermal alteration for immature biomarker molecules. In this study, we develop the kinetics of thermal maturity for long-chain alkenones and plant-wax *n*-alkanes. Plant-wax *n*-alkanes are ubiquitous in Cenozoic (and older) thermally immature sediments [cf., *Brooks and Smith*, 1967] while long-chain alkenones are present in most Neogene marine sediments [*Brassell*, 2014]. This widespread occurrence makes studies of their thermal alteration applicable to most subduction zone settings.

2. Background

2.1. Alkenones

Long-chain unsaturated methyl and ethyl ketones (hereafter alkenones, Figure 1a) are produced by a number of haptophyte algae and are well preserved in ocean sediments [*Herbert*, 2014]. The relative proportion of alkenones with two, three, or four double bonds is thought to be controlled by sea surface temperature (SST) with the level of alkenone unsaturation ($U^{k'}_{37}$) varying linearly with temperature [*Brassell et al*., 1986; *Prahl et al*., 2000]. Hydrous pyrolysis experiments have shown that alkenones thermally mature to an unknown product at temperatures of ~200°C and entirely disappear from the sediment when held at 250°C for 24 h [*Simoneit et al*., 1994]. However, these experiments do not confirm that alkenones react on the shorter timescale associated with earthquakes and other short timescale heating processes. Here, we establish the kinetics of alkenone destruction and the change in $U^{k'}_{37}$ at short timescales.

2.2. *n*-Alkanes

n-Alkanes are linear hydrocarbons (Figure 1b) derived from a wide variety of natural sources. Long-chain *n*-alkanes are found in plant leaf waxes with a preference for odd-over-even chain lengths (Carbon Preference Index—CPI) [*Eglinton and Hamilton*, 2013; *Eglinton et al*., 1962; *Rieley et al*., 1991]. The distribution of *n*-alkane chain lengths is known to change with increasing thermal maturity. Long-chain *n*-alkanes with no carbon preference are formed during kerogen cracking and petroleum formation. With further heating, cracking of the *n*-alkanes themselves reduces the long-chain *n*-alkane abundance [*Eglinton et al*., 1988]. The formation of *n*-alkanes during heating causes the *n*-alkane CPI to decrease, particularly in long chain *n*-alkanes [*Simoneit*, 1994]. These thermal alterations to the *n*-alkane chain length distribution have been studied in experiments on the scale of days [e.g., *Eglinton et al*., 1988]. However, the thermal maturity of *n*-alkanes has not previously been established on shorter timescales relevant to fast geologic heating processes such as earthquakes.

3. Methods

3.1. Hydrous Pyrolysis Experiments

We present a series of hydrous pyrolysis experiments performed on crushed and homogenized samples from deep-sea piston core RC14-99 [*Morley and Heusser*, 1997], taken near to the Japan trench (36°57.9′N, 147°55.7′E, 5652 m depth). This material was selected for its similarity to sediments being subducted in the Japan trench where tsunamigenic earthquakes have occurred [*Maeda et al*., 2011; *Minoura et al*., 2001]. Sediment was sampled from RC14-99, section 6b throughout its depth for three batches (Batch A: 1285–

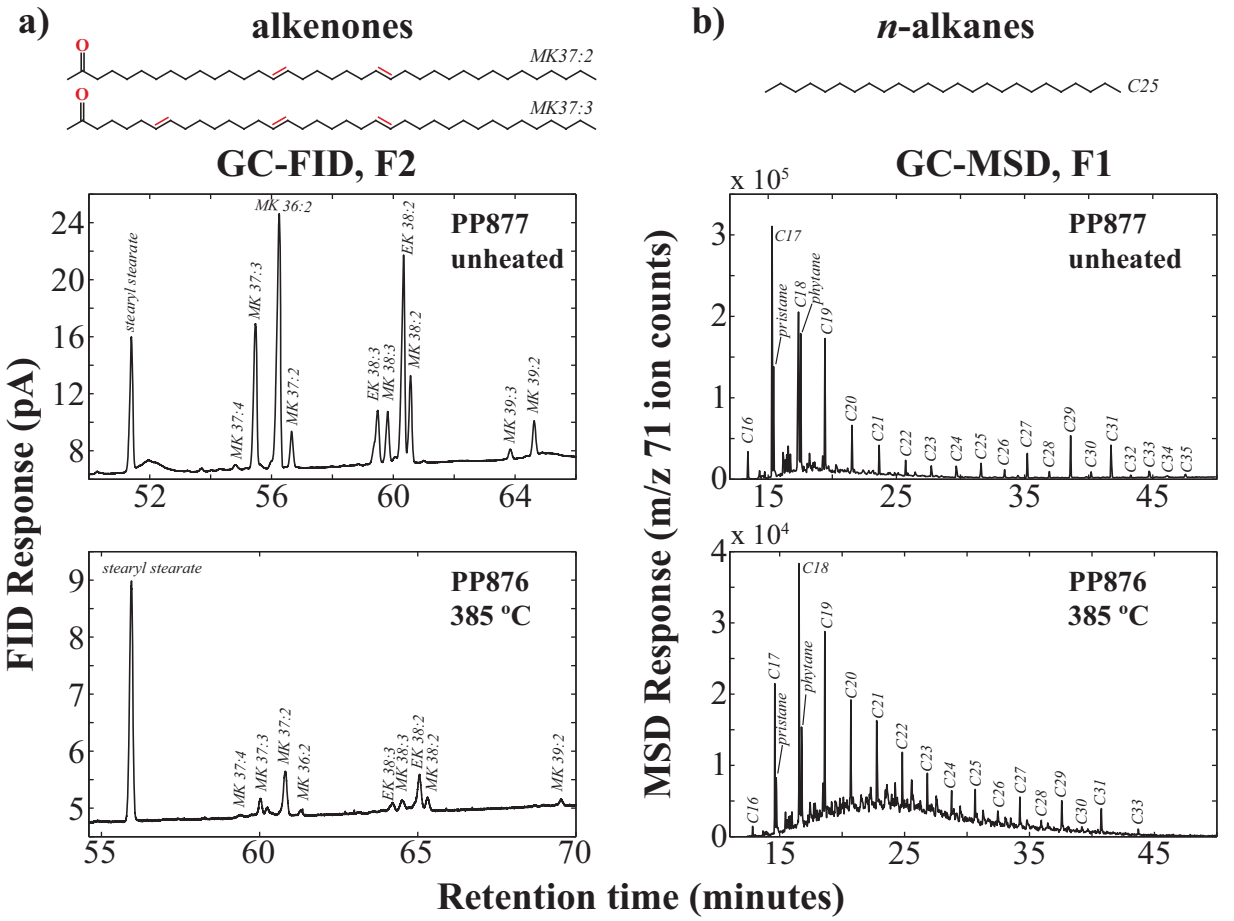

Figure 1. Molecular structure and gas chromatographic analysis of long-chain alkenones and *n*-alkanes. (a) Alkenone concentrations are higher in an unheated sample (PP877) compared to a sample exposed to high temperature (PP876). Alkenone data (a) were collected on a GC-FID with stearyl stearate as an internal recovery standard. Alkenone peaks are labeled as methyl and ethyl ketones with the number of carbon atoms and number of double bonds. (b) *n*-Alkane data were collected on a GC-MSD. Shown are the m/z 71 extracted ion chromatograms that are characteristic for *n*-alkanes. Note that the *n*-alkane internal recovery standard, 5a-androstane, does not have a strong m/z 71 response and is not seen here. Retention times for the unheated and heated samples are slightly different due to slight changes in the column length resulting from column maintenance between run dates.

1405 cm, Batch B: 1280–1436 cm, Batch C: 1244–1454 cm; see supporting information Table S1 for exact sampling depths). Three batches were required due to limitations on the amount of core that we were able to sample with our first two sample requests and because we depleted our initial batches before we had completed our experiments. The core pieces for each batch were crushed with mortar and pestle and mixed to homogenize the sample for the experiments. The prepared sediment was stored in an ashed Fisher 250 mL glass jar, covered with a screw cap lined with ashed foil, and placed in a drawer at room temperature (~20°C) and experimental samples were removed at the time of the experiment using an ashed spatula.

Rapid high-temperature heating experiments were conducted using a small, carburized reactor designed for rapid heating (Figure 2) [*Sheppard et al*., 2015]. To prepare these experiments, 5.0 g of sediment and 6 mL of Fisher Optima-grade ultrapure-deionized water (degassed with N_2 using a sparger) were poured into the reactor. First, about half of the sediment was added, followed by half of the water. The sample was tamped down with a metal push-rod to mix the sediment and water, and then this process was repeated with the remainder of the sediment and water. This procedure prevents unwetted sediment from getting stuck to the bottom of the reactor or floating on top of the water layer. The metal pushrod, reactor, and all other materials that contacted the sample were cleaned with dichloromethane (DCM) and methanol (MeOH) before use.

Once loaded, the reactor was attached to the experimental frame (Figure 2a), evacuated using a vacuum pump, and then pressurized to 1000 psi (6.9 MPa) using He gas to check for leaks. Pressure was reduced to

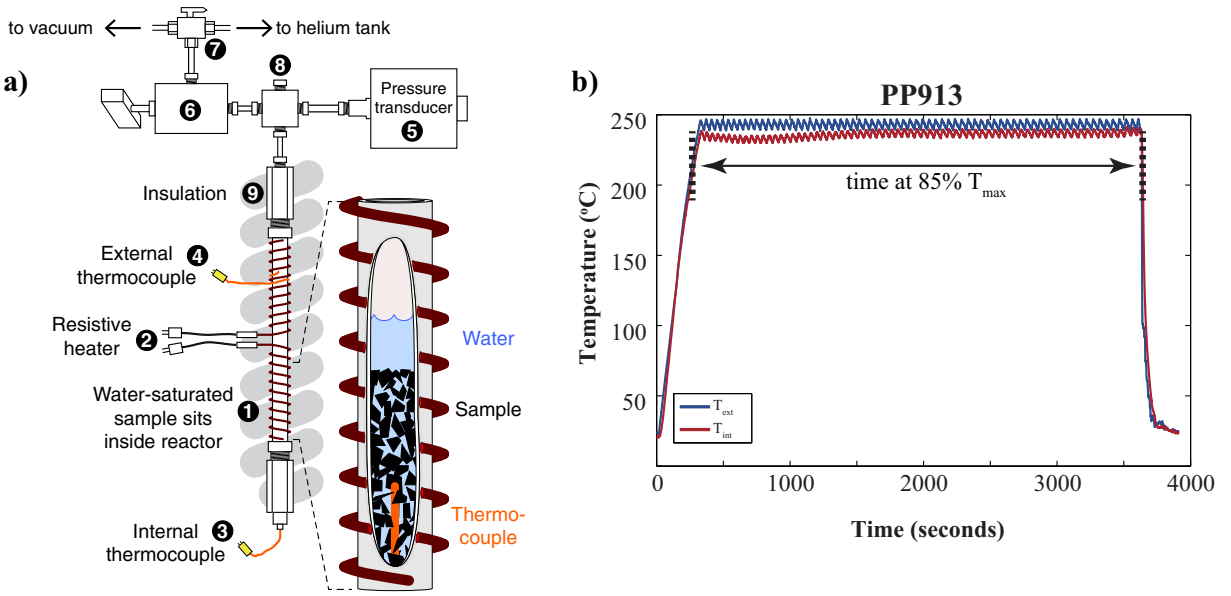

Figure 2. (a) Heating apparatus used in hydrous pyrolysis experiments [after *Sheppard et al*, 2015]. Water and sediment are added to the reactor tube (1) with the internal thermocouple (3) inserted through the bottom fitting. This assembly is then mounted on the experimental frame and is leak-checked by pressurizing to 6895 kPa (1000 psi) of helium (5–8). The tube is then wrapped with a resistive heater (2) and the external thermocouple (4) is placed with its tip to the reactor tube. Finally, the assembly is wrapped with insulation (9). At the end of each experiment, the insulation is unwrapped and the sample is quenched by spraying DI water over the reactor tube.(b) An example of the temperature data collected during the experiments shows the internal and external thermocouple temperatures and typical heating and cooling times. Experiments that experienced peak temperature larger than 30°C above the target temperature and a peak duration longer than 350 s were not used for later calculations in this paper.

10–100 psi of helium (69–690 kPa) prior to a run. Samples were heated using a resistive heater wrapped around the reactor tube. Temperature was measured using an inner thermocouple and an outer thermocouple (Omega J-type thermocouple, maximum temperature range 0–750°C) and controlled using a proportional-integral-derivative (PID) controller. During the experiments, the reactor was wrapped with insulation to allow rapid heating and help maintain temperature. Experiments were conducted at temperatures ranging from 120 to 350°C over durations of 20–180 min (Table 1). Samples achieved experimental temperatures in less than 10 min (Figure 2b). At the end of each experiment, insulation was quickly removed, the resistive heater was unplugged from the PID controller, and the reactor tube was quenched by spraying it with deionized water until the temperature read by the thermocouples was reduced to room temperature. Experiments were quenched in about 1 min (Figure 2b). After the experiment, samples were removed from the reactor using the cleaned push-rod and an ashed (450°C for 8 h) glass fiber filter paper plug (Whatman GF/C) and pushed through into an ashed recovery beaker. The rolled filter paper was necessary to maximize sample recovery by preventing the sample (which had a fine-grained

Table 1. Experimental Conditions for Low Temperature (PP1286–1364) and High Temperature (PP854–1051) Hydrous Pyrolysis Experiments[a]

Purpose	Sample #	Weight (g)[b]	Time (min)[c]	Temp. (°C)[d]	Sediment Batch
Unheated control and alkenone degradation analysis	PP877[e]	4.879		20	A
	PP920[e]	5.006		20	B
	PP1051[e]	5.027		20	A + B
	PP1285[e]	2.003		20	C
	PP1361[e,f]	1.94		20	C
Low temperature thermal alteration	PP1286[g]	1.936	2 h	60	C
	PP1287[g]	1.968	1 day	60	C
	PP1288[g]	1.979	4 days	60	C
	PP1362[g]	1.983	2 h	100	C
	PP1363[g]	1.944	1 day	100	C
	PP1364[g]	2.009	4 days	100	C
High temperature thermal alteration	PP1045	4.701	178.55	124.08	A + B
	PP918	4.969	87.43	132.39	B
	PP873	3.37	28.88	134.25	A
	PP913	4.795	56.25	235.57	B
	PP854	5.077	25.63	237.38	A
	PP917	4.419	83.78	252.94	B
	PP914	4.455	53.93	263.70	B
	PP915	4.639	52.68	308.63	B
	PP875	1.905	22.27	349.97	A
	PP876	1.121	20.07	384.80	A

[a]Sample numbers listed here correspond to sample numbers in Figures 4–7.
[b]Sediment weights measured after sample recovery.
[c]Time at 85% T_{max} in minutes unless otherwise noted
[d]Mean temperature during time at 85% T_{max}.
[e]Sample used as unheated control.
[f]Sample used for alkenone degradation analysis.
[g]Experiments conducted in glass vials in a GC oven.

muddy consistency) from sticking to the reactor walls. The inside of the reactor tube was then rinsed with ultrapure-deionized water into the recovery beaker. Though we were able to recover almost all of the sediment for most experiments (within ~0.5 g of the initial 5 g; Table 1), recovery of sediment from the reactors was sometimes incomplete, yielding variable sample weights for extraction of organic material. The variability in sample recovery was accounted for by reweighing samples after extraction to obtain the weights used in the determination of biomarker concentrations.

Low temperature hydrous pyrolysis experiments were also conducted to constrain the low temperature kinetics of alkenone and *n*-alkane thermal maturity over longer times (Table 1). Our experimental heating setup for the high temperature experiments was not designed for the longer experiments needed to measure reaction kinetics at low temperatures. Therefore, these experiments were conducted in the oven of a gas chromatograph at temperatures of 60 and 100°C and times ranging from 2 h to 4 days. Two-gram samples were placed into 8 mL ashed borosilicate glass vials with 5 mL of degassed ultrapure-deionized water and thoroughly mixed using a spatula cleaned with DCM and MeOH. Vials were purged for 15 s with N_2 gas before being tightly capped. For each set of experiments (at 60 and 100°C), a control vial was left at room temperature for the duration of the experiments. The experimental vials were placed in the oven into a beaker filled with sand that was preheated to the experimental temperature. The sand provided thermal mass to minimize temperature fluctuations when the oven door was opened. In each experiment the temperature was held constant throughout and at each of three predesignated time points (2 h, 1 day, and 4 days), one vial was removed from the oven and quenched by running cold water over the vial until it reached room temperature.

3.2. Total Lipid Extraction

After recovery from the reactor, samples were freeze dried for 1–3 days under a vacuum of 60×10^{-3} mbar. The total lipid extract (TLE) was obtained by sonicating the freeze-dried sediments in a solution of 9:1 DCM: MeOH three times for 15 min. After each sonication, samples were left to settle for 10 min and then the solvent was poured into a 60 mL vial. The experimental samples were too fine grained to decant without pouring significant amounts of sediment into the 60 mL vial during the sonication extractions. Because of this, post-sonication solvent was filtered through an ashed glass fiber filter paper (Whatman GF/F) into the 60 mL recovery vials. We initially used sonication extractions to avoid further heating the sediment during Accelerated Solvent Extraction (ASE) where our standard 100°C method could potentially contaminate the temperature signal from the experiments. However, upon further testing, we found that sonication extraction yielded incomplete recovery of all compounds and that ASE extraction at 100°C effectively extracted all alkenone and alkane molecules. We performed further testing to determine whether ASE extraction altered the distribution and thermal maturity of the extracted compounds in any way. These tests indicated no difference in biomarker signatures in 100°C ASE extractions and multiple, lower temperature extractions of the same material (see supporting information section S1 for more detail).

To ensure complete recovery of organic molecules, samples were extracted a second time using ASE extractions with 9:1 (v/v) DCM:MeOH at an extraction temperature of 100°C. Laboratory recovery standards were added to the collected TLE (5a-androstane and stearyl stearate) and the liquid was evaporated (by a combination of drying in a hood and under a stream of N_2) and then transferred to a 4 mL vial using DCM. Sonication extracted and ASE extracted samples were analyzed separately, with alkenone and *n*-alkane concentrations from the sonication and ASE extractions for each experimental sample summed after measurement. Sonication extractions yielded 40–100% of the total TLE (supporting information Figure S1). Due to some sediment loss in the sonication procedure and the small amount of sediment used in the low temperature hydrous pyrolysis experiments, samples for the 60 and 100°C experiments were only extracted using the ASE method.

3.3. Column Chromatography and Gas Chromatography

The TLE in the 4 mL vial was separated into three fractions (aliphatic, ketone, and polar) using silica gel column chromatography. First, the TLE was brought up in 1 mL hexane and pipetted onto a column containing 0.5 g DCM-rinsed silica gel. An additional 3 mL hexane was then added to the column to elute the F1 (aliphatic) fraction. This procedure was repeated for the F2 (ketone) and F3 (polar) fractions with DCM and MeOH, respectively. The aliphatic and ketone fractions were dried under N_2 and transferred to 2 mL vials with DCM. These were then dried under N_2 and brought up in hexane and toluene, respectively, for analysis

using a gas chromatograph with a flame ionization detector (GC-FID) for the ketone fraction and a gas chromatograph with mass selective detection (GC-MSD) for the aliphatic fraction. Most alkenone samples were run on the GC-FID using the PTV injector with a 60 m DB1 column with a diameter of 0.25 mm and a stationary phase thickness of 0.1μm with a 10 m nonpolar guard column. Samples were injected at a volume of 1 μL. Upon injection, the oven was held at 90°C for 1.5 min, raised to 250°C at a 25°C/min ramp, then raised to 313°C at a 1°C/min ramp and finally raised to 320°C at a 10°C/min ramp and held at 320°C for 20 min. Some of the ketone samples were run using a split-splitless (S/SL) injector with a 60 m VF-200 column (i.d., 0.25 mm, stationary phase thickness 0.1 μm) with a 10 m guard column into which 2 μL of sample was injected. Upon injection, the oven was held at 90°C for 3 min, raised to 250°C at a 25°C/min ramp, then raised to 305°C at a 1°C/min ramp and finally raised to 320°C at a 10°C/min ramp and held at 320°C for 20 min. The samples quantified with the S/SL injector and VF-200 column were analyzed during laboratory testing for the most effective method for alkenone quantification. As described below, we rigorously compared results from the two methods and found no significant differences in alkenone parameters and decided to combine results from the two methods rather than reanalyzing samples run with the S/SL-VF200 method.

We determined the repeatability of measured alkenone parameters with the PTV injector by comparing results from 26 runs of the same F2 ketone fraction acquired over the course of three years. Alkenone concentrations are repeatable within 4.4% and $U^{k'}_{37}$ values were repeatable within 0.006. We also evaluated whether the different injectors and columns produced the same alkenone concentrations and $U^{k'}_{37}$ values. No significant differences were found on measurements of the same samples using the PTV and S/SL injectors (mean difference as a fraction of the sample concentration was $+3.3 \pm 4.4\%$ for concentration and $+0.003 \pm 0.023$ for $U^{k'}_{37}$, N = 8, 1s uncertainties).

The precision of the full analytical procedure (extraction, purification, quantification) was determined by measuring biomarkers in seven aliquots of Batch C sediment extracted on the same day (in order to eliminate the effect of biomarker degradation; see section 4.1 for more discussion) and analyzed together. Total alkenone concentrations (MK37:2 + MK37:3) are repeatable to 4.1% and $U^{k'}_{37}$ values are repeatable to 0.0033. These results are comparable to our long-term GC-FID precision and demonstrate the repeatability of our analyses. Our results for precision on alkenone concentrations and $U^{k'}_{37}$ values are excellent compared to those from a laboratory ring test [*Rosell-Melé et al*., 2001].

n-Alkanes were measured using the GC-MSD run with a multimode inlet and a DB-5 column (30 m length, 0.25 mm i.d., 0.25 μm phase thickness). Sample of 1 μL was injected and the oven held at 60°C for 1.5 min. The temperature was ramped up to 150°C at a rate of 15°C/min and then to 320°C at a rate of 4°C/min where it was held for 10 min. *n*-Alkane chain length distribution parameters are repeatable to $<$1.5% for the CPI and $<$1% for the ADI.

Alkenone chromatograms (Figure 1a) were integrated using ChromQuest software (GC-FID) and *n*-alkane chromatograms (Figure 1b) were integrated using Chemstation software (GC-MSD). Long-chain alkenone peak areas from the ketone fraction were converted to alkenone concentrations (supporting information Table S2) by normalizing to the stearyl stearate internal standard peak area:

$$\left[\frac{ng\ \ molecule}{g\ \ sediment}\right] = \frac{M_{molecule}}{M_{standard}} * \frac{V_{standard} * [standard]}{sample\ \ weight} \quad (1)$$

where $M_{molecule}$ and $M_{standard}$ are the chromatographic peak areas corresponding to the molecule of interest and the standard molecule, respectively, $V_{standard}$ is the volume of recovery standard put into the TLE after extraction (μL), and *[standard]* is the concentration of the standard molecule in the recovery standard (ng/μL).

These concentrations of individual alkenone molecules were used to calculate the total alkenone concentration and $U^{k'}_{37}$ value for each sample (Table 2). Total alkenone concentration was calculated by adding the concentrations of the C_{37} alkenone molecules present in the RC14-99 sediment (MK37:3 and MK37:2). Note that MK37:4 was present in the samples (Figure 1a), but in concentrations too small to reliably quantify. $U^{k'}_{37}$ values were calculated by dividing the concentration of MK37:2 by the summed concentrations of MK37:2 and MK37:3.

Differences in the GC-MSD response for each *n*-alkane were corrected for by analyzing authentic standards with the samples. A mixture of C8–C40 *n*-alkanes plus the 5a-androstane recovery standard was analyzed

Table 2. Biomarker Parameters Measured in Hydrous Pyrolysis Experiments

Sample #	Time (s)[a]	Temperature (°C)[b]	Sediment Batch	Alkenone Conc.	$U^{k'}_{37}$	CPI	ADI
PP877[c]		20	A	1714	0.669	4.29	1.34
PP920[c]		20	B	1517	0.702	4.26	1.32
PP1051[c]		20	A + B	1299	0.714	3.90	1.32
PP1285[c]		20	C	1783	0.654	3.55	1.24
PP1361[c,d]	147 days	20	C	1617	0.665	3.07	1.19
PP1286	7290	60	C	1801	0.652	3.84	1.28
PP1287	86430	60	C	1822	0.653	4.07	1.31
PP1288	345600	60	C	1846	0.647	4.18	1.32
PP1362	7269	100	C	1513	0.662	3.30	1.23
PP1363	86428	100	C	1518	0.659	3.49	1.23
PP1364	345595	100	C	1385	0.6768	3.28	1.23
PP1045	10713	124	A + B	1009	0.728	3.55	1.28
PP918	5246	132	B	1346	0.701	3.94	1.33
PP873	1733	134	A	1107	0.678	3.03	1.20
PP913	3375	236	B	659	0.722	1.96	1.01
PP854	1538	237	A	443	0.681	2.62	1.23
PP917	5027	253	B	298	0.742	3.09	1.23
PP914	3236	264	B	281	0.716	2.28	1.17
PP915	3161	309	B	126	0.775	2.32	1.21
PP875	1336	350	A	484	0.714	2.39	1.15
PP876	1204	385	A	289	0.729	1.77	1.06

[a]Time at 85% T_{max} in seconds unless otherwise noted.
[b]Mean temperature during time at 85% T_{max}.
[c]Sample used as unheated control.
[d]Sample used for alkenone degradation analysis.

with the aliphatic fraction of the samples and used to calculate a GC-MSD relative response factor for each *n*-alkane homologue relative to 5a-androstane. The area ratio of each *n*-alkane molecule to 5a-androstane was then multiplied by this response factor before calculating the concentration by multiplying by the concentration of 5a-androstane in the standard divided by the sample weight (supporting information Table S3). *n*-Alkane concentrations were used to calculate the CPI (odd/even *n*-alkanes from C_{26}–C_{35}) and the ADI (alkane distribution index, $C_{27} + C_{31}/C_{28} + C_{29} + C_{30}$) (Table 2). Here we introduce the ADI index as a measure of the development of a secondary peak in the *n*-alkane chain-length distribution centered on C_{29}. Because this secondary peak develops at a slower rate than the reduction of the CPI or alkenone concentration, an analysis of this change in *n*-alkane distribution can help to place further constraints on coseismic temperature rise.

3.4. Determining the Kinetics of Biomarker Thermal Maturity

The rapid heating of the reactor during our experiments sometimes introduced temperature overshoots that could influence our results. Therefore, temperature data from the experiments were analyzed to ensure that only high-quality isothermal hydrous pyrolysis experiments were used for the determination of the reaction kinetics of alkenone destruction and the change in *n*-alkane distribution. Experiments with an initial peak in temperature that was larger than ~30°C above the eventual steady state temperature and longer in duration than ~350 s were not used in the analysis. Such deviations from isothermal temperature profiles may have occurred due to factors such as variations in the degree of coupling between the resistive heaters and the reactor tube and differences in the wrapping of insulation around the heating apparatus.

After removing nonisothermal experiments, experimental temperatures were determined by taking the mean of the recorded temperature between the time at which the sample achieved 85% of its peak temperature at the beginning of the experiment and the time at which the sample had been cooled down to 85% of its peak temperature at the end of the experiment. Experimental times are considered to be the duration for which the sample was heated to the experimental temperature (Figure 2b). The reaction rate constant, *k*, for isothermal experimental samples was determined by rearranging the following equation [*Lewis*, 1993]:

$$p = 1 - e^{-kt} \quad (2)$$

Table 3. Kinetic Parameters of Thermal Maturity for Biomarkers Determined in This Study

Biomarker Parameter	E (kcal/mol)	A (1/s)	T_{min} (°C)[a]
MK37:2	8.57	1.12	120
MK37:3	8.67	1.39	120
Total alkenone (C_{37})	8.6	1.2	120
CPI	8.08	0.302	120
ADI	7.72	0.052	120

[a]T_{min} is the minimum temperature required to thermally mature biomarkers.

where *p* is the fraction reacted in the given experiment relative to a control sample. Though all experiments were conducted using sediment from RC14-99, we determine the fraction reacted using control samples from the batch of RC14-99 that was used at the same time as each experiment. This allows us to examine the thermal effects on the biomarkers without superimposing signals from differences in the starting biomarker compositions of the batches or any

degradation of the biomarkers resulting from long-term storage at room temperature (see section 4.1). Thus, the controls for the high temperature heating experiments are PP877 (Batch A), PP920 (Batch B), and PP1051 (Batch A+B) for experiment groups PP854–876, PP913–918, and PP1045, respectively. The controls for the low temperature heating experiments are PP1285 and PP1361 for the 60 and 100°C sets, respectively. The fraction reacted value is determined by dividing the measured amount of the given biomarker parameter in each heated sample by the amount in the control sample to obtain the fraction of the parameter remaining (f). This can then be subtracted from 1 to obtain the fraction reacted ($p = 1 - f$). We use the experimentally determined p to obtain an expression for k:

$$k = \frac{-\ln(1-p)}{t}. \tag{3}$$

Experimental values of k were calculated using the p values determined for each experimental sample and the time, t, of each experiment as described above. Using Arrhenius plots, we determined the temperature dependence of kinetic parameters for alkenone destruction and changes in n-alkane distribution by rearranging the Arrhenius equation,

$$k = Ae^{-E_a/RT}, \tag{4}$$

to its linear form:

$$ln(k) = ln(A) - \frac{E_a}{R} * T^{-1}, \tag{5}$$

where A is the preexponential frequency factor (s^{-1}), E_a is the activation energy (kcal/mol), R is the gas constant (1.987×10^{-3} kcal/K*mol), and T is the temperature (K). Using this formulation, $-E_a/R$ is the slope and $ln(A)$ is the intercept of the best-fit line to the Arrhenius plot. Samples with $k<0$ are excluded from the fit. These values result from uncertainty in the measurements themselves and only affect samples heated at the lowest temperatures. An alternative approach involves binning these low temperature experiments and determining the k value from the slope of a best fit line to the t versus $ln(f)$ values for these experiments (supporting information Figure S6). This approach yields similar kinetics for these samples. We also exclude samples PP854 and PP873, which are anomalous for all analyzed biomarkers. This indicates an inaccurate determination of the experimental temperature, possibly resulting from variations in packing the sediment into the reactor for early experiments. Error bounds on the Arrhenius fits are calculated using a Monte Carlo approach as described in *Sheppard et al*. [2015].

4. Results

4.1. Alkenone and $U^{k'}_{37}$ Degradation at Room Temperature

In order to ensure that our estimates of the fractional change in biomarker parameters were not contaminated by a possible signal from interbatch variability, we measured biomarker parameters in control unheated samples during each set of experiments. While we did not observe a consistent interbatch variability in the biomarker parameters (Figure 3), we found that alkenone parameters (total C_{37} concentration and $U^{k'}_{37}$) exhibited significant changes with storage time of the dry sediment on the scale of months to years.

After each sampling of RC14-99 (Batches A, B, and C; supporting information Table S1), the sediment was crushed and combined in an ashed jar (section 3.1). For each set of hydrous pyrolysis experiments, the source batch was sampled until the sediment from that batch was exhausted, at which point, RC14-99 was resampled to make the next batch. This led to three instances of sampling Batch A, and two instances each of sampling Batches B and C for unheated control samples. We also conducted a third sampling of Batch C in which we sampled the batch seven times in one day. This had the additional benefit of demonstrating the precision of the biomarker measurements for different aliquots of the same sample.

We observe a systematic decrease in alkenone concentration and a systematic increase in $U^{k'}_{37}$ with storage time of the crushed dry sediment at room temperature between measurements made months to years apart in all three batches (Figures 3a and 3b). However, the batches did not show a systematic decrease in alkenone concentration or increase in $U^{k'}_{37}$ value as the core aged over the course of this study (i.e., between

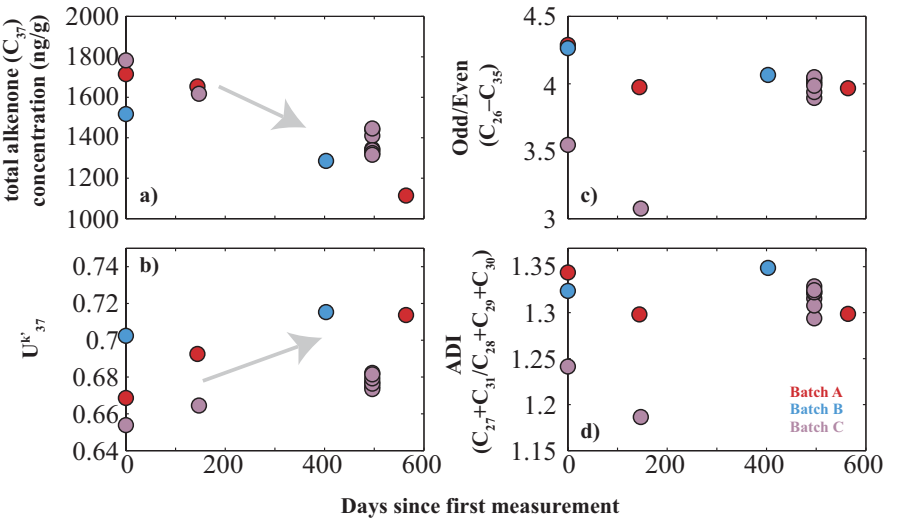

Figure 3. (a) Alkenone concentration, (b) $U^{k'}_{37}$ values, (c) CPI, and (d) ADI measured for each sampled batch of core RC14-99 plotted against the time since the first measurement of the batch. Batch A is red, Batch B is blue, and Batch C is purple. General trends are shown with grey arrows and correspond with the trends observed in the thermal alteration of alkenones (decreasing alkenone concentration and increasing $U^{k'}_{37}$ values). *n*-Alkane indices do not show a consistent trend. The third extraction of Batch C in all parameters shows the samples used to calculate analytical uncertainty.

Batches A, B, and C on their first sampling). Based upon these findings, we control for the effect of storage time by using the control sample analyzed with each group of pyrolysis experiments to normalize our results.

We also measured *n*-alkane concentrations in the control samples over time (Figures 3c and 3d). While there is some scatter in both the CPI and ADI measured at different times in Batch C, Batches A, and B show fairly stable values for these two parameters. We use the control sample of the batch that was extracted at the same time as each set of hydrous pyrolysis experiments to ensure that no potential *n*-alkane degradation overprints the thermal maturity signature.

An important additional observation is that repeat analyses of the same ketone fraction stored in toluene over several years did not show any change in alkenone parameters (section 3.3). This fraction was stored in the dark at 3°C (37°F) when not being analyzed. This finding indicates that the change in alkenone parameters we observed with dry storage of crushed sediment is specifically related to either the sediment matrix or storage conditions and is not a process operating universally during storage of alkenone molecules. Furthermore, the observations that the initial alkenone parameters for each successive sediment batch did not systematically change and that the sediment core itself had any alkenones preserved indicates that the degradation process is either accelerated or activated by the crushing and storage of the sediment samples after sampling the core.

4.2. Alkenone Destruction

Hydrous pyrolysis experiments show that alkenone concentration decreases over short time periods at high temperatures (Figure 4a). Low temperature hydrous pyrolysis experiments conducted at 60°C demonstrate that there is no measureable change in alkenone concentration at these temperatures, even over long periods of time (Figure 4a). Shorter experiments conducted above 120°C show significant change in alkenone concentration (Figure 4a). Long-duration experiments conducted at 100°C show a slight decrease in alkenone concentration; however, the reaction rate calculated for these experiments is lower than would be predicted from an Arrhenius fit to the higher temperature experiments, implying a change in mechanism (Figure 4b). As a result, the Arrhenius fit for alkenones (Figure 4b) only includes experiments above 120°C. From this fit, we obtain values for E_a and A of 8.6 kcal/mol and 1.2 s^{-1}, respectively.

There is also an increasing trend in the proportion of di to triunsaturated alkenones with higher temperatures and longer duration experiments. We report these changes using the $U^{k'}_{37}$ parameter typically used for paleoceanographic reconstruction of sea surface temperatures. The $U^{k'}_{37}$ parameter is defined as:

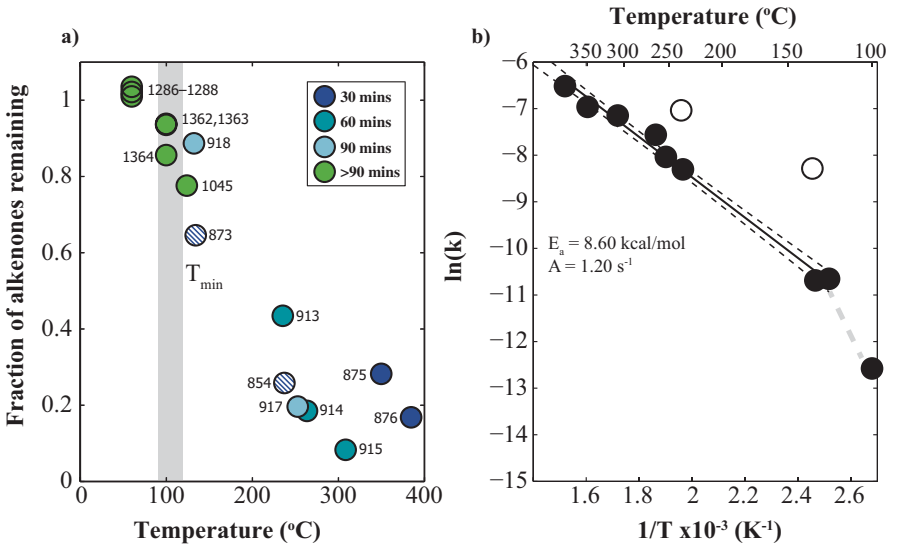

Figure 4. (a) Alkenone concentration decreases with increasing temperature over various durations. Long experiments (green) were conducted over 2 h to 4 days. (b) Arrhenius relationship of alkenone destruction showing the natural log of the reaction rate (k) plotted against inverse temperature in K. The linear fit demonstrates a first-order Arrhenius relationship. A clear difference in the reaction rate-temperature relationship occurs below 120°C and, thus only experiments ≥ 100°C are used to calculate the kinetic parameters of alkenone destruction. Hatched points (a) or open points (b) correspond to samples that exhibited anomalous results for all biomarker parameters are not used in the fit.

$$U^{k\prime}_{37} = \frac{MK37:2}{MK37:2 + MK37:3} \tag{6}$$

where MK37:2 and MK37:3 are methyl ketones with 37 C atoms and 2 or 3 unsaturated bonds, respectively. In the case of $U^{k'}_{37}$, the values increase with increasing thermal maturity (Figure 5a). The increase in $U^{k'}_{37}$ is accompanied by a marked decrease in both the MK37:2 and MK37:3 concentrations (Figure 5b). The decrease in the concentration of these two molecules also becomes most notable at temperatures above ~120°C. Arrhenius analysis of MK37:2 and MK37:3 shows that the kinetics of destruction for these individual alkenone molecules are nearly identical to the kinetics of destruction calculated for the total alkenone concentrations with E_a values for MK37:2 and MK37:3 of 8.57 and 8.67 kcal/mol and A values of 1.12 and 1.39 s^{-1}, respectively. However, while the rates for MK37:2 and MK37:3 destruction are similar at lower temperatures, the MK37:3 destruction rate increases more at higher temperatures leading to greater destruction and an increase in the $U^{k'}_{37}$ value (Figure 5b). As the rate of $U^{k'}_{37}$ change will depend upon the relative concentrations of MK37:2 and MK37:3 initially present in the sediment (Figure 5d), it is more appropriate to use the individual kinetics of each alkenone molecule to interpret change in $U^{k'}_{37}$ values for samples that have a different starting $U^{k'}_{37}$ value from our sample material (see supporting information section S2 for more details).

4.3. *n*-Alkane Distribution

There are significant changes in the distribution of *n*-alkanes in our experiments (Figures 6a and 7a) as the biogenic signature in the long-chain *n*-alkane distributions of the unheated sediment are overprinted. We see a decrease in the odd/even preference in the long-chain *n*-alkanes and increasing amounts of mid-chain *n*-alkanes with no odd/even preference (supporting information Figure S5). We examine two particular parameters that capture different trends in this distribution change. First, we focus on the Carbon Preference Index (CPI), which is defined as the ratio between the odd chain length and even chain length *n*-alkanes from C_{26}–C_{35}. We see a decrease in CPI with increasing temperature, beginning at temperatures of ~120°C (Figure 6a). We determine the kinetics of reduction in CPI using an Arrhenius analysis, fitting experiments above 120°C, and obtain values for E_a and A of 8.08 kcal/mol and 0.302 s^{-1}, respectively (Figure 6b).

While the decrease in odd/even preference is directly measured in the CPI, we also observe the creation of low CPI long-chain *n*-alkanes with a maximum at C_{29} unlike the preexisting *n*-alkanes in the sample, which

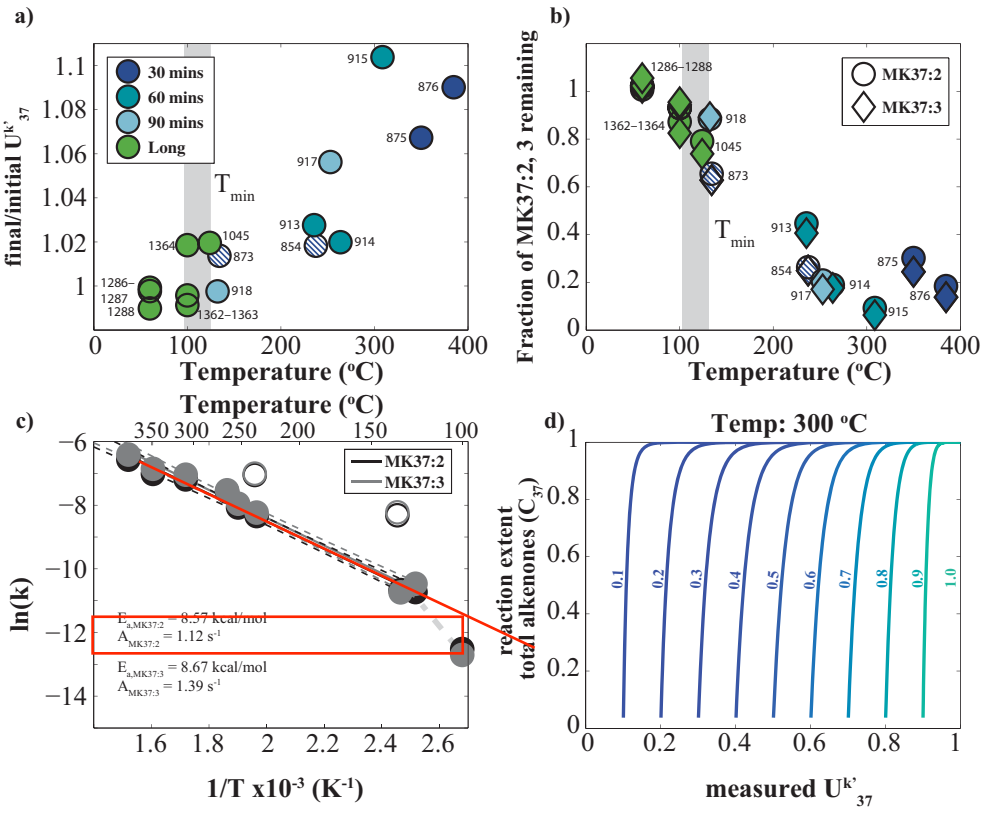

Figure 5. (a) $U^{k'}_{37}$ change (final $U^{k'}_{37}$ value/initial $U^{k'}_{37}$ value) is positively correlated with temperature. (b) MK37:2 and MK37:3 concentrations decrease with increasing temperature, though MK37:3 decreases more dramatically. (c) Arrhenius relation for MK37:2 and MK37:3. In Figures 5a–5c, hatched (a and b) and hollow points (c) correspond to samples not used in the fit. (d) Examples of heating paths at 300°C for samples with different initial $U^{k'}_{37}$ values. Each curve shows the $U^{k'}_{37}$ values as total alkenone destruction proceeds. At low to moderate alkenone reaction extents (0 to 0.8), the change in $U^{k'}_{37}$ is greatest for initial $U^{k'}_{37}$ values near 0.5. At very high alkenone reaction extents the $U^{k'}_{37}$ changes are greater for initial $U^{k'}_{37}$ near zero.

have a maximum at C_{31}. To track the combined effects of this process, we also introduce the *n*-alkane distribution index (ADI), defined as:

$$ADI = \frac{C_{27} + C_{31}}{C_{28} + C_{29} + C_{30}} \tag{7}$$

This parameter describes a relative change in long chain-length *n*-alkanes in the range of C_{28}–C_{30} with respect to the surrounding chain lengths with increasing temperature (Figure 7c). The ADI decreases as low CPI *n*-alkanes are created during heating and the average *n*-alkane chain length decreases, leading to the creation of *n*-alkanes with a maximum around C_{29}. The ADI shows a decrease with increasing time and temperature (Figure 7b), predominantly observed at temperatures above 120°C. However, in this case, the scatter of the ADI values calculated for individual experiments at 120–135°C includes one sample with a slight increase in ADI, indicating that this temperature range is very close to the minimum temperature at which reaction might be expected. We determine the values of E_a and A for the thermal alteration of the ADI to be 7.72 kcal/mol and 0.052 s^{-1}, respectively.

4.4. Sulfur Concentration

Although not the main focus of the work presented here, we note an increase in the concentration of solvent-extractable elemental sulfur detected in the highest temperature experiments (supporting information Figure S4). Present as S_8 in the solvent extract, this product presumably reflects breakdown of other sulfur phases in the sediments at high temperature. Further studies with more high temperature experiments are required to understand the reactions occurring and to determine kinetics based on this change (see supporting information section S3).

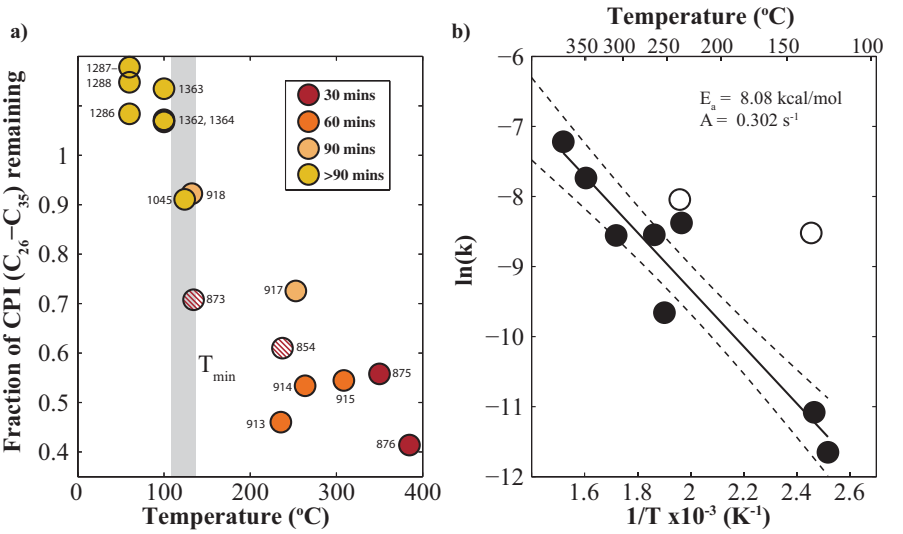

Figure 6. (a) CPI (odd/even chain length *n*-alkanes C_{26}–C_{35}) for hydrous pyrolysis experiments presented in this study. We see a decrease in CPI with increasing temperature, though the decrease is mostly apparent above 120°C. (b) Arrhenius relation for the CPI degradation rate constants. (a) Hatched and (b) hollow points correspond to samples not used in fit.

5. Discussion

5.1. Kinetics of Biomarker Thermal Maturity

Our experiments exhibit first-order reaction kinetics whose temperature dependence can be described by an Arrhenius-type relationship (Figures 4–7b). We further find that within experimental uncertainty there is no destruction of alkenones below temperatures of ~60°C (Figure 4a). Our low temperature experiments were run for up to 4 days to specifically investigate low temperature reactions. The lack of reaction in our long, 60°C experiments and the small amount of reaction in the 100°C experiments is not predicted from the higher temperature experiments and thus indicates a change in the temperature dependence of the reaction rate at low temperatures. Quantification of this change in temperature dependence will require an additional suite of experiments.

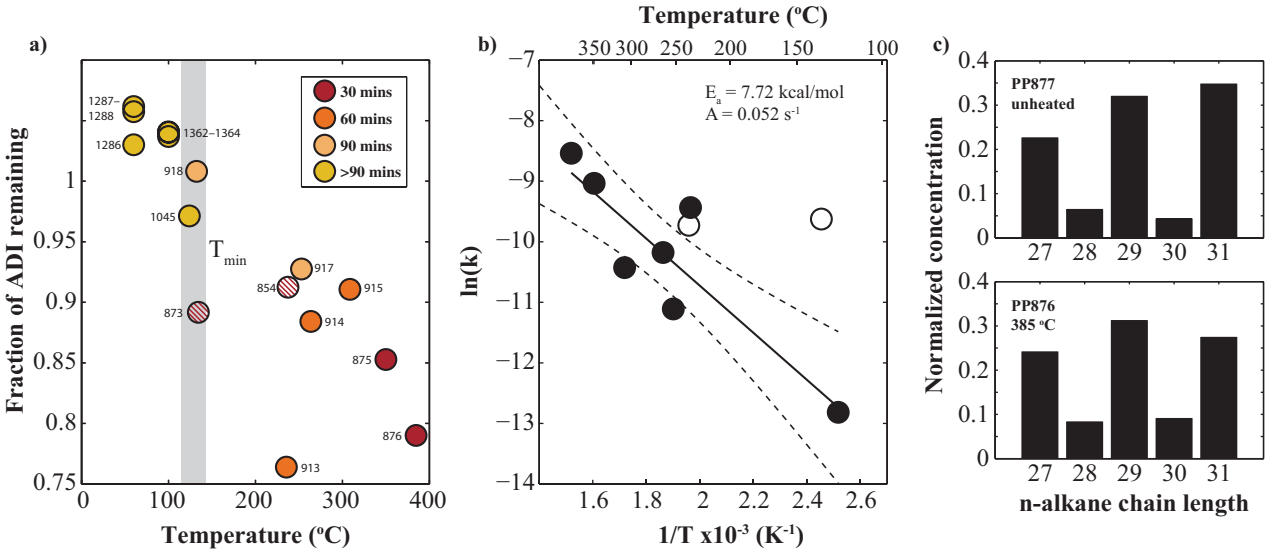

Figure 7. (a) Change in the *n*-alkane distribution index (ADI) with increasing temperature for hydrous pyrolysis experiments in this study. (b) Arrhenius plot for the ADI. (c) Histograms of C27–C31 *n*-alkane concentrations, normalized to the sum of C27–C31, for the sample heated to 385°C (PP876) and the corresponding control (PP877). (a) Hatched and (b) hollow points correspond to samples not used in fit.

We also observe differences in the reaction rate of the di and triunsaturated C_{37} methyl ketones. The reaction rate for the triunsaturated ketone is slightly greater, especially at higher temperatures, producing an increase in the $U^{k'}_{37}$ value with reaction extent. Changes in $U^{k'}_{37}$ could thus provide additional information on alkenone destruction independent of total alkenone concentration. This could be particularly beneficial as the precision and accuracy during measurement of the $U^{k'}_{37}$ index is better than for the total alkenone concentration (section 3.3) [*Rosell-Melé et al*., 2001]. The extent of $U^{k'}_{37}$ change with heating temperature (T) and time (t) also depends upon the initial $U^{k'}_{37}$ value:

$$U^{k'}_{37}(t,T) = \frac{1}{1+\left[\frac{1}{U^{k'}_{37,0}}-1\right] * e^{(k_2(T)-k_3(T))t}} \quad (8)$$

where $U^{k'}_{37}(t)$ and $U^{k'}_{37,0}$ are the final and initial $U^{k'}_{37}$ values, respectively, and k_2 and k_3 are the temperature-dependent reaction rate constants from MK37:2 and MK37:3, respectively (see supporting information section S2 for more detail). This relationship allows an estimate of the fractional change in MK37:2 or MK37:3 in a heated sample by comparing the measured $U^{k'}_{37}$ value with an initial $U^{k'}_{37}$ value.

The only previous work on thermal alkenone destruction we can compare our results with is *Simoneit et al*. [1994]. They investigated the destruction of long-chain unsaturated alkenones in sediments from Middle Valley, in the north of the Juan de Fuca ridge system (ODP Leg 139). Their hydrous pyrolysis experiments, conducted at temperatures of 200–350°C over 24 h demonstrated complete destruction of alkenones at 250°C and partial destruction at 200°C. Interestingly, they found that the $U^{k'}_{37}$ value decreased from an initial value of 0.81–0.69 in the 200°C experiment with partial alkenone destruction. We see the $U^{k'}_{37}$ value systematically increasing in all of our heated experiments in a manner consistent with slight differences in the rate constants for the MK37:2 and MK37:3 molecules. At this point we do not know the reason that the $U^{k'}_{37}$ value decreased in the *Simoneit et al*. [1994] experiments but increased in our experiments. Attack of the double bond positions is one pathway for alkenone destruction and would favor greater destruction of the triunsaturated molecule as found in our experiments.

While thermal maturity in alkenones is largely expressed as a change in absolute concentration, the thermal maturity of *n*-alkanes is observed as a change in chain length distribution (Figure 1b). We see a reduction in CPI at temperatures above 120°C, consistent with previous observations of the changes in *n*-alkane chain length distribution [*Eglinton et al*., 1988; *Simoneit*, 1994]. This is indicative of overprinting of the biogenic signature for a strong preference for odd chain-lengths, derived from plant leaf waxes [*Eglinton et al*., 1962] by petrogenic hydrocarbons with a CPI of ~1. The change in *n*-alkane distribution is also described by a decrease in the ADI. This parameter is representative of an increase in the C_{28}–C_{30} *n*-alkane concentration compared to the surrounding chain lengths (Figure 7c). This transition is likely caused by the superimposed effects of the formation of long chain *n*-alkanes due to high temperature cracking reactions, the breakdown of these long-chain *n*-alkanes to form shorter-chain molecules, and the reduction of odd chain lengths with respect to even chain lengths (supporting information Figure S5). Because this parameter describes multiple processes, the observed change in ADI yields a strong signal with increasing thermal maturity.

Figure 8 shows the Arrhenius relationships for the biomarkers analyzed in this study (Figure 8a) and the predicted time-temperature values for samples that have experienced 5% biomarker reaction. Changes at this scale should be easily detectable given the precision of our measurements for all biomarker parameters discussed in this study, even with variable initial biomarker values. Notably, the kinetics of thermal maturity differs significantly between the alkenones and *n*-alkanes with the former reacting more quickly at lower temperatures (Figure 8a). Additionally, these kinetic parameters are quite different from those previously determined for methylphenanthrenes [*Sheppard et al*., 2015], indicating a higher reaction rate, but lower temperature sensitivity for biomarkers present in fresh sediments compared with biomarkers generated as a result of burial heating (Figure 8a). These results provide tantalizing evidence for a dramatic divergence in the kinetics of thermal maturation for different biomarker parameters. By measuring biomarker parameters with different kinetics in a heated sample, we gain better constraints on the possible time-temperature combinations that a sample has experienced.

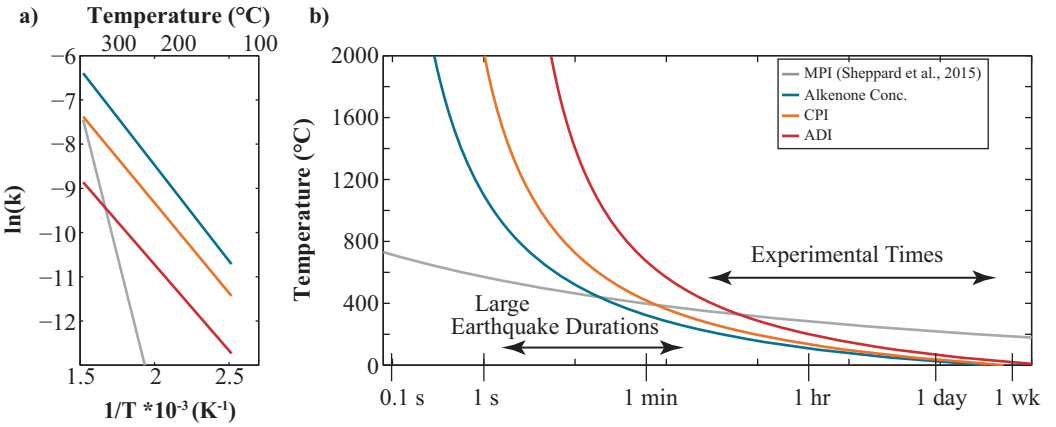

Figure 8. (a) Arrhenius best-fit line for all compound parameters analyzed in this study. Methylphenanthrene kinetics (MPI-1) are from *Sheppard et al*. [2015]. (b) Time-temperature diagram illustrating where 5% reaction occurs in each biomarker parameter. Time-temperature combinations above these curves should be detectable using these biomarker heating proxies.

5.2. Application as Fault Thermometers

We observe significant changes in concentration for marine and terrigenous organic material in short-duration hydrous pyrolysis experiments. This suggests that the thermal maturity of biomarkers can be used to estimate temperature rise on faults hosted in unaltered marine sediments. This is particularly of interest for shallow faults active in subduction zones where large amounts of shallow slip can significantly enhance the tsunamigenic potential of a subduction zone margin [*Fujii et al*., 2011]. In these types of environments, thermal alteration of biomarkers in unaltered sediments can provide a constraint on coseismic temperature rise, which, in turn, can help to constrain the coseismic stress conditions that govern the propagation of shallow seismic slip. This is particularly important because subduction zones host the largest earthquakes due to the large amount of fault area available for slip relative to other tectonic environments.

The differences in kinetic parameters of thermal maturity in these biomarkers have the potential to provide added constraints on the maximum temperature rise experienced by marine sediments hosting seismic faults. This is because sediment that has experienced a given time-temperature history will record different degrees of alteration in the alkenone and *n*-alkane parameters. By constraining the degree of alteration of a suite of biomarkers, more precise estimates of temperature rise can be made than are possible using only one biomarker. By coupling thermal diffusion models with the kinetics for different biomarkers, a more thorough understanding of the coseismic temperature rise and subsequent temperature decay during earthquakes can be achieved. We note that the kinetics of thermal maturation analyzed in this paper is unlikely to be of use in sediments containing methylphenanthrenes. This is because, if the sediments are thermally mature enough to contain methylphenanthrenes, the *n*-alkanes are likely to have experienced enough thermal alteration to overprint the original biogenic fingerprint. Thus, in order to use the thermal maturity of *n*-alkanes to help constrain temperature rise on faults in sediments that have experienced burial heating, more experiments on sediment with a more thermally mature initial composition are required.

In order to accurately assess thermal alteration in sediments, it is of utmost importance to fully characterize the initial biomarker parameters of the unheated protolith. Concentrations of different biomarkers can vary widely over short stratigraphic intervals and throughout the oceans. Therefore it is important to establish the natural variability within the protolith in order to confidently attribute anomalies to temperature rise. In settings such as subduction zones, initial concentrations can be measured in input sediments on the downgoing plate, as long as independent parameters are used to assess stratigraphic equivalence. For instance, *Rabinowitz et al*. [2015] showed that trace element geochemistry could be used to correlate stratigraphy between a core through the Japan trench décollement and a nearby reference core.

5.3. Implications of Biomarker Degradation for Sediment Sampling and Storage

Our observations of significant alteration in alkenone concentration and *n*-alkane distribution with heating suggest that care should be taken when using samples that may have experienced heating (e.g., around faults or hydrothermal areas) for paleoclimatological studies. Notably, we observe a systematic difference in

the kinetics of thermal maturity between alkenone molecules with different levels of unsaturation. This implies that samples that have been exposed to heating above 120°C, even for a short amount of time, such as might be expected in a faulted or hydrothermal environment, should not be relied upon for representative $U^{k'}_{37}$ values. However, our long-duration experiments at 60°C show no significant change in $U^{k'}_{37}$ value. We therefore suggest that samples exposed to such low levels of heating might retain their biogenic $U^{k'}_{37}$ values although extrapolation to thousands or millions of years of burial includes large uncertainties from our kinetic parameters. In addition, the observed changes in the distribution of *n*-alkane chain lengths due to heating support the conclusion that care should be taken when interpreting *n*-alkane data in hydrothermal and faulted areas [e.g., *Simoneit*, 1994].

We further observe the degradation of alkenone concentration and $U^{k'}_{37}$ values in our crushed control samples stored at room temperature over the span of months to years. Because the batches each sampled slightly different parts of core RC14-99 6b, variation in both initial alkenone concentration and $U^{k'}_{37}$ is to be expected between starting materials. If alkenone degradation were taking place while the samples were still in the core, this trend might be expected to dominate any climatically controlled interbatch variability. In addition, if alkenone degradation in the cores was as dramatic as we observe in our control sediment, we might expect all alkenones to be destroyed in cores that have been stored at room temperatures for decades (as has core RC14-99, which was recovered in 1972). Since the presence of alkenones in our experimental sediment belies this possibility, we suggest that the degradation of alkenones in our control samples over the span of months to years occurred postcrushing and could be related to the resultant higher surface area of the sediment that is exposed to atmospheric conditions (e.g., higher oxidation).

6. Conclusions

Hydrous pyrolysis experiments conducted on Western Pacific sediment allow us to determine the kinetics of thermal maturation for a suite of biomarker parameters found in marine sediments, specifically alkenone destruction, increase in $U^{k'}_{37}$, and transformation of the plant-wax *n*-alkane signature to a petrogenic distribution observed as reductions in the CPI and ADI (*n*-alkane distribution index, $C_{27} + C_{31}/(C_{28} + C_{29} + C_{30})$). These thermal maturation kinetics can be used to constrain the temperature rise on seismic faults in marine environments and allow for a more thorough understanding of shallow seismic slip.

Acknowledgments
Samples for this study were provided by the Lamont-Doherty Core Repository. We thank two anonymous reviewers for helpful comments. Funding for this project was provided by U.S. National Science Foundation grant OCE 12-60555, a Schlanger Ocean Drilling Fellowship to H.S.R., part of the NSF-sponsored U.S. Science Support Program for IODP that is administered by the Consortium for Ocean Leadership, Inc., and an NSF GRFP (DGE-11-44155) to H.S.R. Data used in this paper can be found in the supporting information Tables. LDEO Contribution No. 8083

References

Barker, C. E., and M. J. Pawlewicz (1986), The correlation of vitrinite reflectance with maximum temperature in humic organic matter, in *Lecture Notes in Earth Sciences, Paleogeothermics*, edited by G. Buntebarth and L. Stegena, pp. 79–93, Springer, Berlin.

Bishop, A. N., and G. D. Abbott (1993), The interrelationship of biological marker maturity parameters and molecular yields during contact metamorphism, *Geochim. Cosmochim. Acta*, *57*(15), 3661–3668, doi:10.1016/0016-7037(93)90147-O.

Bowden, S. A., R. W. Court, D. Milner, E. C. Baldwin, P. Lindgren, I. A. Crawford, J. Parnell, and M. J. Burchell (2008), The thermal alteration by pyrolysis of the organic component of small projectiles of mudrock during capture at hypervelocity, *J. Anal. Appl. Pyrol.*, *82*(2), 312–314, doi:10.1016/j.jaap.2008.05.002.

Brassell, S.C., R. G. Brereton, G. Eglinton, J. Grimalt, G. Liebezeit, I. T. Marlowe, U. Pflaumann, and M. Sarnthein (1986), Palaeoclimatic signals recognized by chemometric treatment of molecular stratigraphic data, *Org. Geochem.*, *10*(4), 649–660, doi:10.1016/S0146-6380(86)80001-8.

Brassell, S. C. (2014), Climatic influences on the Paleogene evolution of alkenones, *Paleoceanography*, *29*, 255–272, doi:10.1002/2013PA002576.

Brooks, J. D., and J. W. Smith (1967), The diagenesis of plant lipids during the formation of coal, petroleum and natural gas-I. Changes in the n-paraffin hydrocarbons, *Geochim. Cosmochim. Acta*, *31*(12), 2389–2397, doi:10.1016/0016-7037(67)90010-5.

Burnham, A. K., J. Sweeney, and L. Livermore (1989), A chemical kinetic model of vitrinite maturation and reflectance, *Geochim. Cosmochim. Acta*, *53*(10), 2649–2651, doi:10.1016/0016-7037(89)90136-1.

Collettini, C., C. Viti, T. Tesei, and S. Mollo (2013), Thermal decomposition along natural carbonate faults during earthquakes, *Geology*, *41*(8), 927–931, doi:10.1130/G34421.1.

D'Alessio, M. A., A. E. Blythe, and R. Burgman (2003), No frictional heat along the San Gabriel fault, California: Evidence from fission-track thermochronology, *Geology*, *31*(6), 541–544, doi:10.1130/0091-7613(2003)031 < 0541:NFHATS>2.0.CO;2.

Di Toro, G., R. Han, T. Hirose, N. De Paola, S. Nielsen, K. Mizoguchi, F. Ferri, M. Cocco, and T. Shimamoto (2011), Fault lubrication during earthquakes, *Nature*, *471*(7339), 494–498, doi:10.1038/nature09838.

Eglinton, G., and R. J. Hamilton (2013), Leaf epicuticular waxes, *Science*, *156*(3780), 1322–1335, doi:10.1126/science.156.3780.1322.

Eglinton, G., A. G. Gonzalez, R. J. Hamilton, and R. A. Raphael (1962), Hydrocarbon constituents of the wax coatings of plant leaves: A taxonomic survey, *Phytochemistry*, *1*(2), 89–102, doi:10.1016/S0031-9422(00)88006-1.

Eglinton, T. I., A. G. Douglas, and S. J. Rowland (1988), Release of aliphatic, aromatic and sulphur compounds from Kimmeridge kerogen by hydrous pyrolysis: A quantitative study, *Org. Geochem.*, *13*(4), 655–663, doi:10.1016/0146-6380(88)90086-1.

Fujii, Y., K. Satake, S. Sakai, M. Shinohara, and T. Kanazawa (2011), Tsunami source of the 2011 off the Pacific coast of Tohoku Earthquake, *Earth Planets Space*, *63*(7), 815–820, doi:10.5047/eps.2011.06.010.

Fulton, P. M., and R. N. Harris (2012), Thermal considerations in inferring frictional heating from vitrinite reflectance and implications for shallow coseismic slip within the Nankai Subduction Zone, *Earth Planet. Sci. Lett.*, *335*, 206–215, doi:10.1016/j.epsl.2012.04.012.
Han, R., T. Shimamoto, T. Hirose, J. H. Ree, and J. I. Ando (2007), Ultralow friction of carbonate faults caused by thermal decomposition, *Science*, *316*(5826), 878–881, doi:10.1126/science.1139763.
Herbert, T. D. (2014), Alkenone paleotemperature determinations, in *Treatise on Geochemistry*, 2nd ed., vol. 8, edited by H. D. Holland and K. K. Turekian, pp. 399–433, Elsevier, Oxford doi:10.1016/B978-0-08-095975-7.00615-X.
Hirono, T., et al. (2007), A chemical kinetic approach to estimate dynamic shear stress during the 1999 Taiwan Chi-Chi earthquake, *Geophys. Res. Lett.*, *34*, L19308, doi:10.1029/2007GL030743.
Kaiho, K., S. Yatsu, M. Oba, P. Gorjan, J. Casier, and M. Ikeda (2013), A forest fire and soil erosion event during the Late Devonian mass extinction Brussels Late Devonian, *Palaeogeogr. Palaeoclimatol. Palaeoecol.*, *392*, 272–280, doi:10.1016/j.palaeo.2013.09.008.
Kirkpatrick, J. D., and C. D. Rowe (2013), Disappearing ink: How pseudotachylytes are lost from the rock record, *J. Struct. Geol.*, *52*, 183–198, doi:10.1016/j.jsg.2013.03.003.
Lewis, C. A. (1993), The kinetics of biomarker reactions: Implications for the assessment of the thermal maturity of organic matter in sedimentary basins, in *Organic Geochemistry*, edited by M. H. Engel and S. A. Macko, pp. 491–510, Plenum, New York.
Maeda, T., T. Furumura, S. Sakai, and M. Shinohara (2011), Significant tsunami observed at ocean-bottom pressure gauges during the 2011 off the Pacific coast of Tohoku Earthquake, *Earth Planets Space*, *63*(7), 803–808, doi:10.5047/eps.2011.06.005.
Mase, C. W., and L. Smith (1985), Pore-fluid pressures and frictional heating on a fault surface, *Pure Appl. Geophys.*, *122*(2), 583–607, doi:10.1007/BF00874618.
Minoura, K., F. Imamura, D. Sugawara, Y. Kono, and T. Iwashita (2001), The 869 Jogan tsunami deposit and recurrence interval of large-scale tsunami on the Pacific coast of northeast Japan, *J. Nat. Disaster Sci.*, *23*(2), 83–88.
Morley, J. J., and L. E. Heusser (1997), Role of orbital forcing in east Asian monsoon climates during the last 350 kyr: Evidence from terrestrial and marine climate proxies from core RC14-99, *Paleoceanography*, *12*(3), 483–493, doi:10.1029/97PA00213.
Parnell, J., G. R. Osinski, P. F. Green, and M. J. Baron (2005), Thermal alteration of organic matter in an impact crater and the duration of postimpact heating, *Geology*, *33*(5), 373–376, doi:10.1130/G21204.1.
Parnell, J., S. Bowden, P. Lindgren, M. Burchell, D. Milner, M. Price, E. C. Baldwin, and I. A. Crawford (2010), The preservation of fossil biomarkers during meteorite impact events: Experimental evidence from biomarker-rich projectiles and target rocks, *Meteorit. Planet. Sci.*, *45*(8), 1340–1358, doi:10.1111/j.1945-5100.2010.01100.x.
Peters, K. E., C. C. Walters, and J. M. Moldowan (2004), *The Biomarker Guide*, Cambridge Univ. Press, Cambridge, U. K.
Polissar, P. J., H. M. Savage, and E. E. Brodsky (2011), Extractable organic material in fault zones as a tool to investigate frictional stress, *Earth Planet. Sci. Lett.*, *311*(3), 439–447, doi:10.1016/j.epsl.2011.09.004.
Prahl, F., T. Herbert, S. C. Brassell, N. Ohkouchi, M. Pagani, D. Repeta, A. Rosell-Melé, and E. Sikes (2000), Status of alkenone paleothermometer calibration: Report from Working Group 3, *Geochem. Geophys. Geosyst.*, *1*(11), 1034, doi:10.1029/2000GC000058.
Rabinowitz, H. S., H. M. Savage, T. Plank, J. D. Kirkpatrick, and C. D. Rowe (2015), Multiple major faults at the Japan Trench: Chemostratigraphy of the plate boundary at IODP Exp. 343: JFAST, *Earth Planet. Sci. Lett.*, *423*, 57–66, doi:10.1016/j.epsl.2015.04.010.
Rice, J. R. (2006), Heating and weakening of faults during earthquake slip, *J. Geophys. Res.*, *111*, B05311, doi:10.1029/2005JB004006.
Rieley, G., R. J. Collier, D. M. Jones, G. Eglinton, P. A. Eakin, and A. E. Fallick (1991), Sources of sedimentary lipids deduced from stable carbon-isotope analyses of individual compounds, *Nature*, *352*, 425–427, doi:10.1038/352425a0.
Rosell-Melé, A., et al. (2001), Precision of the current methods to measure the alkenone proxy Uk'37 and absolute abundance in sediments: Results of an interlaboratory comparison study, *Geochem. Geophys. Geosyst.*, *2*(7), 1046, doi:10.1029/2000GC000141.
Rowe, C. D., and W. A. Griffith (2015), Do faults preserve a record of seismic slip: A second opinion, *J. Struct. Geol.*, *78*, 1–26, doi:10.1016/j.jsg.2015.06.006.
Sakaguchi, A., et al. (2011), Seismic slip propagation to the updip end of plate boundary subduction interface faults: Vitrinite reflectance geothermometry on Integrated Ocean Drilling Program NanTro SEIZE cores, *Geology*, *39*(4), 395–398, doi:10.1130/G31642.1.
Savage, H. M., P. J. Polissar, R. E. Sheppard, C. D. Rowe, and E. E. Brodsky (2014), Biomarkers heat up during earthquakes: New evidence of seismic slip in the rock record, *Geology*, *42*(2), 99–102, doi:10.1130/G34901.1.
Schimmelmann, A., M. Mastalerz, L. Gao, and P. E. Sauer (2009), Dike intrusions into bituminous coal, Illinois Basin: H, C, N, O isotopic responses to rapid and brief heating, *Geochim. Cosmochim. Acta*, *73*(20), 6264–6281, doi:10.1016/j.gca.2009.07.027.
Schleicher, A. M., A. Boles, and B. A. van der Pluijm (2015), Response of natural smectite to seismogenic heating and potential implications for the 2011 Tohoku earthquake in the Japan Trench, *Geology*, *43*(9), 755–758, doi:10.1130/G36846.1.
Sheppard, R. E., P. J. Polissar, and H. M. Savage (2015), Organic thermal maturity as a proxy for frictional fault heating: Experimental constraints on methylphenanthrene kinetics at earthquake timescales, *Geochim. Cosmochim. Acta*, *151*, 103–116, doi:10.1016/j.gca.2014.11.020.
Sibson, R. H. (1975), Generation of pseudotachylyte by ancient seismic faulting, *Geophys. J. Int.*, *43*(3), 775–794, doi:10.1111/j.1365-246X.1975.tb06195.x.
Simoneit, B. R. T. (1994), Lipid/bitumen maturation by hydrothermal activity in sediments of Middle Valley, Leg 139, in *Proceedings of the Ocean Drilling Program, Scientific Results*, edited by M. J. Mottl et al., pp. 447–465, Ocean Drill. Program, College Station, Tex.
Simoneit, B. R. T., F. G. Prahl, R. N. Leif, and S.-Z. Mao (1994), Alkenones in sediments of Middle Valley, Leg 139: Application as thermal sensors, in *Proceedings of the Ocean Drilling Program, Scientific Results*, edited by M. J. Mottl et al., pp. 479–484, Ocean Drill. Program, College Station, Tex.
Yang, T., M. J. Dekkers, and B. Zhang (2016), Seismic heating signatures in the Japan Trench subduction plate-boundary fault zone: Evidence from a preliminary rock, *Geophys. J.*, *205*(1), 332–344, doi:10.1093/gji/ggw013.